THE JOURNAL OF PHYSICAL CHEMISTRY B

 VOLUME 104, NUMBER 6, FEBRUARY 17, 2000

LETTERS

Reverse Micelle Synthesis and Characterization of Superparamagnetic $MnFe_2O_4$ Spinel Ferrite Nanocrystallites

Chao Liu, Bingsuo Zou, Adam J. Rondinone, and Z. John Zhang*

School of Chemistry & Biochemistry, Georgia Institute of Technology, Atlanta, Georgia 30332-0400

Received: October 5, 1999; In Final Form: November 18, 1999

$MnFe_2O_4$ nanoparticles are synthesized by using sodium dodecylbenzenesulfonate (NaDBS) to form water-in-toluene reverse micelles. The nanoparticles are single crystalline, and the average particle size can be controlled from 4 to 15 nm. High- and low-resolution transmission electron microscopy characterization has shown that the nanoparticles can have a size distribution as narrow as ~9%. Neutron diffraction and magnetic measurements have been conducted on the nanoparticles with a diameter of 7.7 ± 0.7 nm. The results unambiguously prove that these $MnFe_2O_4$ nanoparticles are truly superparamagnetic. The synthesis and characterization of these nanoparticles will facilitate the development of $MnFe_2O_4$ nanoparticles for the potential applications such as contrast enhancement agents of magnetic resonance imaging and magnetic carriers for site-specific drug delivery.

Superparamagnetism as a unique feature of magnetic nanocrystals is of great interest in basic science such as macroscopic quantum tunneling of spin states.[1,2] Also, superparamagnetic nanoparticles can have broad applications including ferrofluid technology,[3] contrast enhancement of magnetic resonance imaging (MRI),[4] and magnetically guided site-specific drug delivery.[5] Spinel ferrites, MFe_2O_4 (M = Mn, Co, Ni, Cu, Zn, Mg, or Cd, etc.) are among the most important magnetic materials and have been widely used for electronic applications over the past half century.[6,7] The great tunability in chemical composition and bonding makes spinel ferrites excellent candidates for understanding and controlling the magnetic properties of nanoparticles through the variation of chemistry at the atomic level. Magnetic nanoparticles with excellent and controllable superparamagnetic properties can be developed from spinel ferrites.

One of most common spinel ferrites, $MnFe_2O_4$ nanoparticles have attracted broad attention because of their potentials as contrast enhancement agents in MRI technology.[8−13] Although some spinel ferrite nanoparticles have been synthesized by various methods,[14−18] there is a lack of synthetic methods for making high quality $MnFe_2O_4$ nanoparticles over a large size range with a narrow size distribution.[19−21] We have developed a reverse micelle method to synthesize $MnFe_2O_4$ nanoparticles that have a controllable size from about 4 nm to 15 nm. The size distribution is usually about 15% although it can be as narrow as ~9%. The superparamagnetic properties of these $MnFe_2O_4$ nanoparticles have been characterized by using SQUID magnetometry and neutron diffraction.

$MnFe_2O_4$ nanoparticles are synthesized through the formation of water-in-toluene reverse micelles with sodium dodecylbenzenesulfonate (NaDBS) $[CH_3(CH_2)_{11}(C_6H_4)SO_3]Na$ as surfactant. The synthesis starts with 0.005 mol of $Mn(NO_3)_2$ and 0.01 mol of $Fe(NO_3)_3$ dissolved in 25 mL of water to form a clear solution. A 0.4 M NaDBS aqueous solution (25 mL) is added into the metal salt solution and followed by the addition of a large volume of toluene. The volume ratio of water and toluene determines the size of $MnFe_2O_4$ nanoparticles. For obtaining the nanoparticles with a size of ~8 nm, the ratio is 5/100 for

* Author to whom correspondence should be addressed.

10.1021/jp993552g CCC: $19.00
Published on Web 01/20/2000

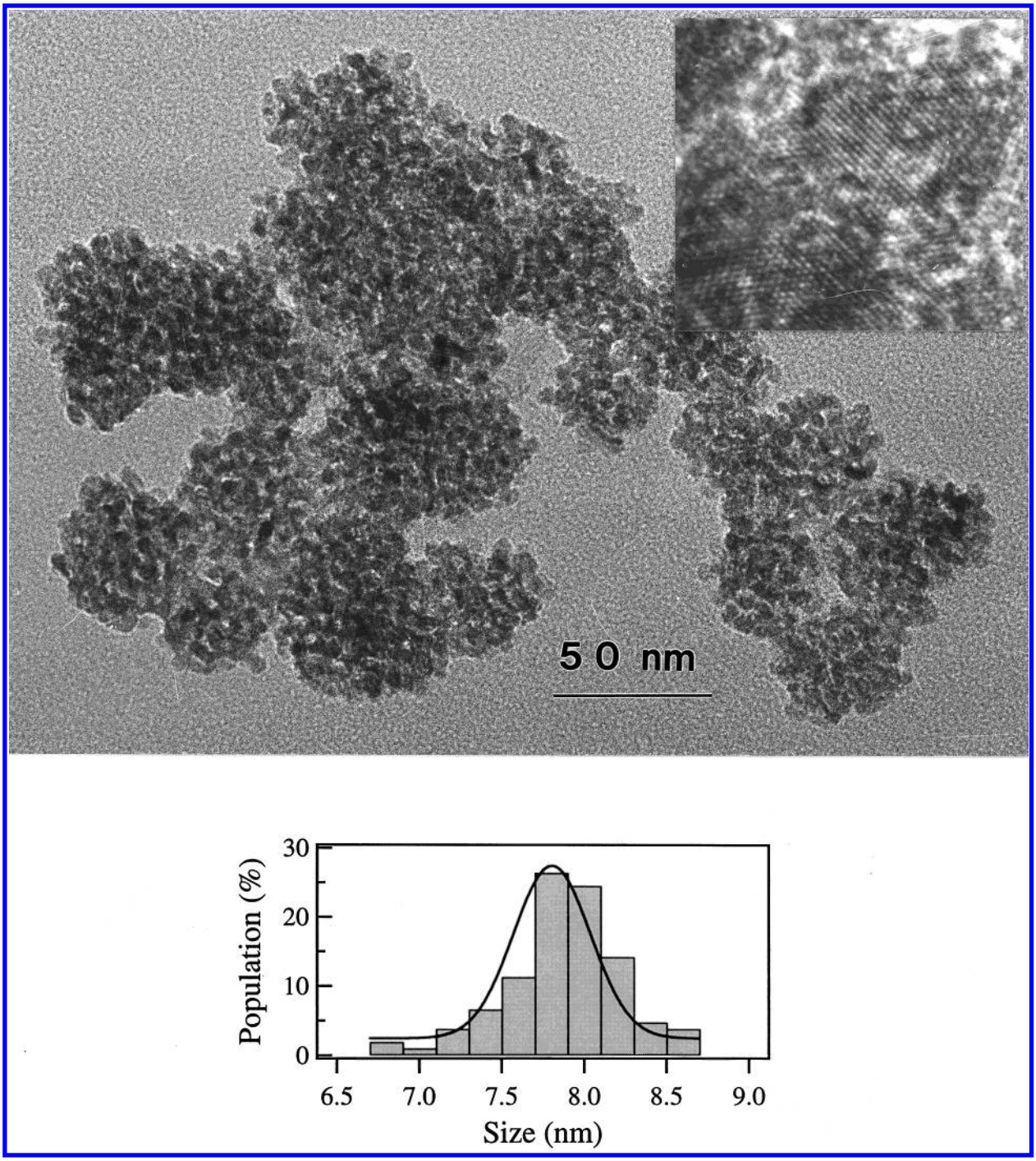

Figure 1. Transmission electron micrograph (200K magnification) of $MnFe_2O_4$ nanoparticles with a size of 7.7 ± 0.7 nm and the particle diameter histogram. The inset is the micrograph at 1500K magnification.

water to toluene. After stirring overnight, the mixture becomes a clear single-phase solution containing reverse micelles. To form colloids in reverse micelles, 40 mL of 1.0 M NaOH aqueous solution is added drop by drop accompanied by vigorous stirring. The solution is stirred for two more hours to complete the formation of colloids. Then, the volume of the solution is reduced by distilling out water and most of the toluene solvent. The concentrated solution with suspended colloids is washed with water and ethanol to remove excess surfactant. The products are collected through centrifugation. X-ray diffraction shows that the samples are in amorphous phase at this stage.

After heat treatment at 350 °C for 12 h under He atmosphere, the nanocrystallites are formed. X-ray diffraction identifies these samples as pure $MnFe_2O_4$ spinel nanoparticles. Elemental analysis by an inductively coupled plasma (ICP) method confirms that Mn to Fe has a 1:2 ratio. The average size of the nanoparticles has been calculated from the peak broadening in X-ray diffraction pattern by using the Debye−Scherrer equation.

Low- and high-resolution transmission electron microscopy (TEM) has been used to confirm the nanoparticle size and to determine the particle size distribution. The nanoparticles under TEM show a narrow size distribution. Figure 1 displays the TEM micrograph of the $MnFe_2O_4$ nanoparticles with a size of 7.7 ± 0.7 nm, which is consistent with the average size obtained from the peak broadening in X-ray diffraction studies. Such consistence implies that the $MnFe_2O_4$ nanoparticles are single crystalline. The size distribution has been determined from the

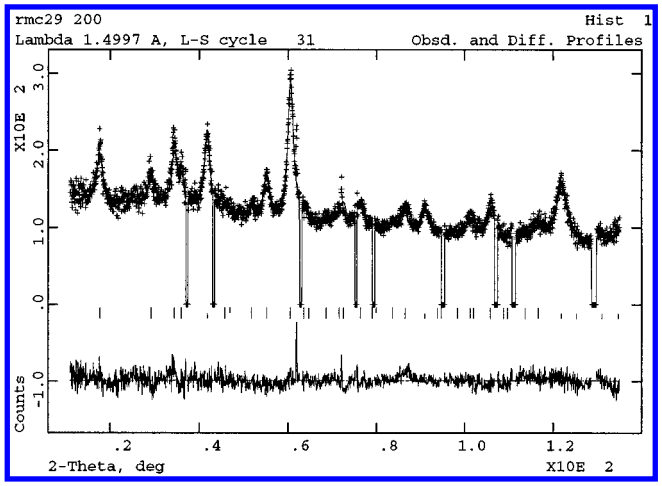

Figure 2. Neutron diffraction patterns of ~8 nm $MnFe_2O_4$ nanoparticles at 200 °C. The "goodness of fit", χ^2, is 2.07. Below the pattern, the first row of the sticks marks the peaks from the magnetic scattering of $MnFe_2O_4$ nanoparticles. The second row of the sticks corresponds to the peaks from the nuclear scattering. The excluded regions (downward sparks) eliminate the diffraction peaks of the Al container.

diameter histogram obtained by statistically measuring the size of more than one hundred individual nanoparticles. The high-magnification TEM image shows clearly the lattice fringes of these nanocrystallites (inset in Figure 1).

Spinel ferrite such as $MnFe_2O_4$ usually has its cations of Mn^{2+} and Fe^{3+} distributed among its tetrahedral A sites and octahedral B sites. One clear understanding of the cation distribution is essential since the magnetic properties of $MnFe_2O_4$ nanoparticles are greatly affected by the cation distribution.[22] Neutron diffraction is used to determine the Mn and Fe cation distribution between A and B lattice sites in spinel unit cell. Figure 2 displays the neutron diffraction pattern of ~8 nm size $MnFe_2O_4$ nanoparticles at 200 °C. The Rietveld refinement shows that the magnetic sublattices are well ordered with an antiferromagnetic alignment, which is consistent with the ferrimagnetic nature of $MnFe_2O_4$ spinel ferrites. Refinement by only considering nuclear scattering could not fit satisfactorily with all the diffraction peaks. The nanoparticles have a mixed spinel structure with a formula of $Mn_{0.45}Fe_{0.55}(Mn_{0.29}Fe_{0.71})_2O_4$ where the cations in parentheses occupy the octahedral sites of the unit cell. The lattice constant for the cubic spinel unit cell is 8.4447(9) Å at 200 °C. Magnetic moment is 1.82 μ_B at the tetrahedral A sites and −2.46 μ_B at the octahedral B sites.

The magnetic properties of the $MnFe_2O_4$ nanoparticles are studied by a SQUID magnetometer (Quantum Design MPMS-5S). Figure 3 shows the temperature dependence of magnetization and remanent magnetization decay (thermal remanent magnetization) of the $MnFe_2O_4$ nanoparticles. The $MnFe_2O_4$ nanoparticles for temperature-dependent magnetization study is cooled from room temperature to 5 K under a zero magnetic field. After a magnetic field of 100 G is applied at 5 K, the magnetization of the nanoparticles is measured as temperature increases. The magnetization increases initially as the temperature rises from 5 K (ZFC in Figure 3). A maximum is reached around 150 K, and then the magnetization starts to decrease with increasing temperature. In the studies of the temperature dependence of remanent magnetization decay, the $MnFe_2O_4$ nanoparticles are cooled from room temperature to 5 K under a magnetic field of 100 G. After the magnetic field is turned off, the remanent magnetization is recorded at temperatures from 5 to 350 K. The remanent magnetization decreases rapidly with increasing temperature (TRM in Figure 3). It approaches zero when the temperature rises to about 150 K.

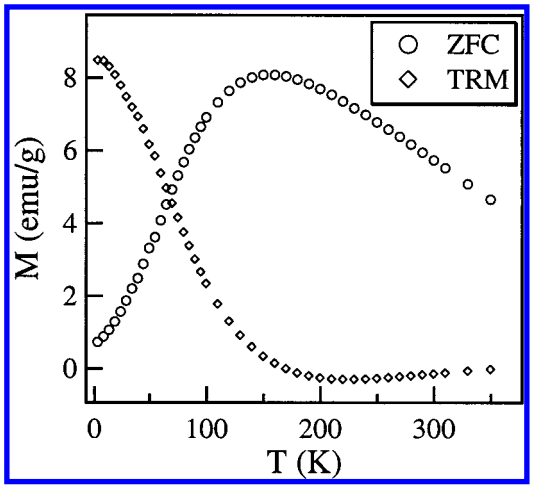

Figure 3. Temperature dependence of remanent magnetization decay for ~8 nm $MnFe_2O_4$ nanoparticles cooled under a magnetic field of 100 G (TRM), and temperature dependence of the magnetization under a magnetic field of 100 G for zero-field-cooled ~8 nm $MnFe_2O_4$ nanoparticles (ZFC).

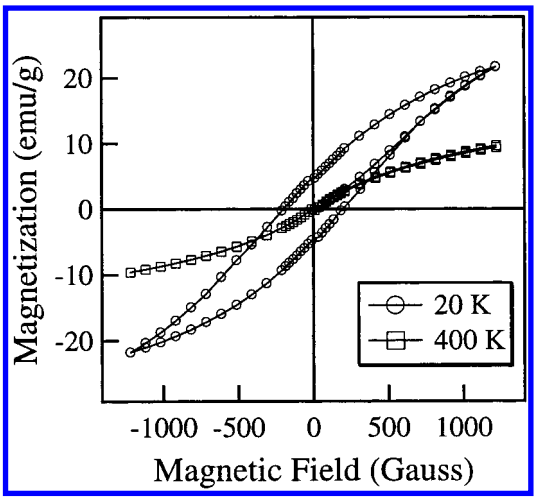

Figure 4. Magnetization vs applied magnetic field for the $MnFe_2O_4$ nanoparticles with a diameter of ~8 nm.

The magnetic field dependence of the magnetization of $MnFe_2O_4$ nanoparticles is shown in Figure 4. The magnetization of the nanoparticles at 20 K has a hysteresis feature. The coercivity of the nanoparticles at that temperature is about 190 G. When the measuring temperature rises above 150 K, the hysteresis feature in the magnetization of the $MnFe_2O_4$ nanoparticles disappears. The field-dependent magnetization plot at 400 K in Figure 4 displays that the magnetization of the nanoparticles changes directions in unison with the direction reversal of the applied magnetic field.

The studies of neutron diffraction and the temperature-dependent decay of remanent magnetization characterize the superparamagnetic nature of these $MnFe_2O_4$ nanoparticles.[23−25] $MnFe_2O_4$ nanoparticles have a Curie transition temperature, T_c around 300 °C.[22] Below T_c, the magnetic moments of $MnFe_2O_4$ align in an antiferromagnetic order. When the $MnFe_2O_4$ nanoparticles are cooled below the blocking temperature without a magnetic field, all the net magnetic moments in each single-domain $MnFe_2O_4$ nanoparticle point along their easy axis to achieve a local minimum of potential energy. Magnetic anisotropy acts as an energy barrier to prevent the magnetization direction switching away from the easy axis of a nanoparticle. The random packing of the nanoparticles results in the overall random-pointed magnetization direction of individual nanopar-

SCHEME 1

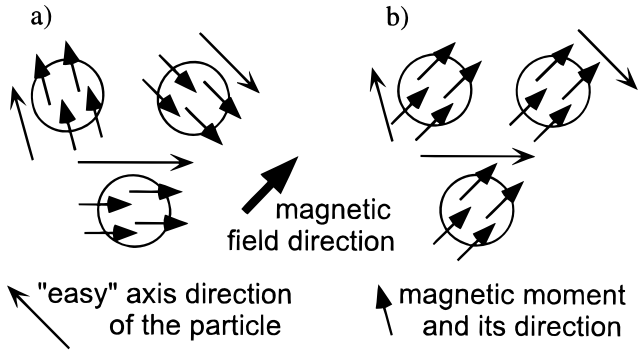

ticle at 5 K as shown in Scheme 1a. The total magnetization of the $MnFe_2O_4$ nanoparticles is almost zero at 5 K since the applied magnetic field is not strong enough to overcome the magnetic anisotropy alone (ZFC in Figure 3). When temperature rises, the magnetic anisotropy in some nanoparticles is overcome and the magnetization directions of these thermally activated nanoparticles start to align with the applied field as a typical paramagnetic material does. Therefore, the total magnetization initially increases with increasing temperature. When the temperature reaches the blocking temperature, the magnetization directions of almost all of the nanoparticles point to the field direction and give a high magnetization reading. As the temperature increases above the blocking temperature, the sample follows a typical paramagnetic behavior of decreasing magnetization versus increasing temperature although the possible weak interparticle interaction may alter their paramagnetic behavior slightly. As a result, a maximum magnetization occurs around the blocking temperature.[26]

When a 100 G magnetic field is applied during the cooling process in the measurement of remanent magnetization, all the net magnetic moments of the $MnFe_2O_4$ nanoparticles are aligned along the field direction regardless of the easy axis direction of each individual nanoparticle. As the nanoparticles are cooled to 5 K, the magnetization direction of each particle is frozen to the field direction as shown in Scheme 1b. Although the magnetic field is turned off at 5 K, the energy barrier from magnetic anisotropy blocks any change of the magnetization direction. The anisotropy energy barriers usually have a broad distribution in random-oriented nanoparticulate samples for many reasons including the size distribution and the distribution of the angles between the easy axis and the direction of the applied magnetic field.[26] As the temperature rises, the nanoparticles with lower magnetic anisotropy get thermally activated. The magnetic directions of these nanoparticles fluctuate and give a time-averaged zero magnetization. Consequently, the remanent magnetization starts to decrease (TRM in Figure 3). The magnetic anisotropy in almost all of the nanoparticles is thermally overcome at 150 K, and the remanent magnetization approaches zero. At temperatures above 150 K, the $MnFe_2O_4$ nanoparticles show no remanent magnetization as the same as paramagnetic materials.[27] Nevertheless, neutron diffraction shows that the $MnFe_2O_4$ nanoparticles have a well-defined magnetic order even at a temperature as high as 200 °C. These results unambiguously demonstrate that these are truly superparamagnetic nanoparticles. The blocking temperature for ~8 nm $MnFe_2O_4$ nanoparticles is 150 K.

During the field-dependent magnetization measurement at 20 K, the thermal activation energy is very low. The change in the magnetization direction of the $MnFe_2O_4$ nanoparticles requires an energy input from the applied magnetic field. When the direction of the field is just reversed, the magnetization direction of the nanoparticles stays along the same direction due to the energy confinement by the anisotropy energy barrier. When the field strength increases to reach the coercive field, the energy barrier is overcome and the magnetization direction of the $MnFe_2O_4$ nanoparticles turns to rendezvous with the applied field. The anisotropy energy barrier has already been overcome by the thermal activation above the blocking temperature, and there is no energy blocking to prevent the change in the magnetization direction of the nanoparticles. Therefore, the magnetization direction changes simultaneously with the reversal of the applied field at 400 K (Figure 4).

In summary, we have shown that $MnFe_2O_4$ nanoparticles with narrow size distribution can be synthesized through water-in-toluene reverse micelles formed by NaDBS surfactant. Neutron diffraction and various magnetic measurements unambiguously show that these $MnFe_2O_4$ nanoparticles are truly superparamagnetic. We are currently studying the size effect to the superparamagnetic properties of $MnFe_2O_4$ nanoparticles and the correlation between the superparamagnetic properties and the magnetic anisotropy barriers in various-sized $MnFe_2O_4$ nanoparticles. These studies will surely facilitate the understanding and controlling of the magnetic properties of nanoparticles. Furthermore, these studies provide an excellent superparamagnetic nanoparticulate system for developing contrast enhancement agents of MRI and magnetic carriers for site-specific drug delivery.

Acknowledgment. We thank Dr. Bryan Chakoumakos of Oak Ridge National Laboratory for his help in neutron diffraction studies. A.J.R. is partially supported by a Cherry Henry Emerson Chemistry Fellowship and a Molecular Design Institute Fellowship. We gratefully acknowledge the financial support in part from NSF (DMR-9875892) and the Beckman Young Investigator program of the Arnold and Mabel Beckman Foundation. The neutron diffraction studies were carried out at Oak Ridge National Laboratory, which is managed by Lockheed Martin Energy Research Corp. for the U.S. Department of Energy under contract number DE-AC0596OR22464.

References and Notes

(1) Awschalom, D. D.; DiVincenzo, D. P. *Phys. Today* **1995**, *48* (4), 43.
(2) Tejada, J.; Ziolo, R. F.; Zhang, X. X. *Chem. Mater*. **1996**, *8*, 1784.
(3) Raj, K.; Moskowitz, R.; Casciari, R. *J. Magn. Magn. Mater*. **1995**, *149*, 174.
(4) Mitchell, D. G. *J. Magn. Reson. Imaging* **1997**, *7*, 1.
(5) Pulfer, S. K.; Gallo, J. M. In *Scientific and Clinical Applications of Magnetic Carriers*; Häfeli, U., Schütt, W., Teller, J., Zborowski, M., Eds.; Plenum Press: New York, 1997; p 445.
(6) Gillot, B. *Eur. Phys. J. AP* **1998**, *4*, 243.
(7) Sugimoto, M. *J. Am. Ceram. Soc.* **1999**, *82*, 269.
(8) Tang, Z. X.; Sorensen, C. M.; Klabunde, K. J.; Hadjipanayis, G. C. *Phys. Rev. Lett.* **1991**, *67*, 3602.
(9) Kulkarni, G. U.; Kannan, K. R.; Arunarkavalli, T.; Rao, C. N. R. *Phys. Rev. B* **1994**, *49*, 724.
(10) Van der Zaag, P. J.; Noordermeer, A.; Johnson, M. T.; Bongers, P. E. *Phys. Rev. Lett.* **1992**, *68*, 3112.
(11) Brabers, V. A. M. *Phys. Rev. Lett.* **1992**, *68*, 3113.
(12) Van der Zaag, P. J.; Brabers, V. A. M.; Johnson, M. T.; Noordermeer, A.; Bongers, P. E. *Phys. Rev. B* **1995**, *51*, 12009.
(13) Gillot, B.; Laarj, M.; Kacim, S. *J. Mater. Chem.* **1997**, *7*, 827.
(14) Moumen, N.; Pileni, M. P. *Chem. Mater*. **1996**, *8*, 1128.
(15) Pileni, M. P.; Moumen, N. *J. Phys. Chem*. **1996**, *100*, 1867.
(16) Perez, J. A. L.; Quintela, M. A. L.; Mira, J.; Rivas, J.; Charles, S. W. *J. Phys. Chem. B* **1997**, *101*, 8045.
(17) Chen, Q.; Zhang, Z. J. *Appl. Phys. Lett*. **1998**, *73*, 3156.
(18) Chen, Q.; Rondinone, A. J.; Chakoumakos, B. C.; Zhang, Z. J. *J. Magn. Magn. Mater*. **1999**, *194*, 1.
(19) Tang, Z. X.; Sorensen, C. M.; Klabunde, K. J.; Hadjipanayis, G. C. *J. Colloid Interface Sci.* **1991**, *146*, 38.

(20) Seip, C. T.; Carpenter, E. E.; O'Connor, C. J.; John, V. T.; Li, S. *IEEE Trans. Magn.* **1998**, *34*, 1111.

(21) Zhang, Z. J.; Wang, Z. L.; Chakoumakos, B. C.; Yin, J. S. *J. Am. Chem. Soc.* **1998**, *120*, 1800.

(22) Chen, J. P.; Sorensen, C. M.; Klabunde, K. J.; Hadjipanayis, G. C.; Devlin, E.; Kostikas, A. *Phys. Rev. B* **1996**, *54*, 9288.

(23) Aharoni, A. *Introduction to the Theory of Ferromagnetism*; Oxford University Press: New York, 1996; p 92.

(24) Stoner, E. C.; Wohlfarth, E. P. *Philos. Trans. R. Soc. A* **1948**, *240*, 599; reprinted in *IEEE Trans. Magn.* **1991**, *27*, 3475.

(25) Leslie-Pelecky, D. L.; Rieke, R. D. *Chem. Mater.* **1996**, *8*, 1770.

(26) Rondinone, A. J.; Samia, A. C. S.; Zhang, Z. J. *J. Phys. Chem. B* **1999**, *103*, 6876.

(27) Chantrell, R. W.; El-Hilo, M.; O'Grady, K. *IEEE Trans. Magn.* **1991**, *27*, 3570.